

Distributed Malfunction Estimation of Multi-Area Interconnected Power Systems Based on Intermediate Observer and Multi-Agent Systems

Ziming Wang, Zhao Zhang, Hongyan Zhou, and Xue-Bo Chen

Abstract—This paper designs a multi-agent-based intermediate observer for malfunction and state estimation of a multi-area interconnected power system. By building a simplified linear model of the power systems, a distributed malfunction observer based on intermediate variables is designed to achieve the estimation of actuator and sensor malfunction signals while considering the system's own and neighboring output estimation errors. The method overcomes the dependence of the conventional observer on the matching condition of the observer and calculates the gain of the observer by solving the linear matrix inequality. Eventually, through an example of simulation, the effectiveness of the design is verified.

Index Terms—power systems, multi-agent systems, intermediate observer, malfunction estimation, linear matrix inequality.

I. INTRODUCTION

FREQUENCY is the key parameter of maintaining power system stability. Frequency fluctuations are severe and can cause frequency deviation. The long-term effects of deviations can cause contact line overloads and damage to generators and other equipment. For multi-area interconnected power systems (IPS), frequency control is important to ensure that the frequency fluctuates within the appropriate range and to keep the deviation of the exchange power of the contact line within the set limits. Therefore, load Frequency Control (LFC) is remarkable and research value to ensure stabilization of the power system. [1, 2].

In the past years, the researchers have presented many results of LFC strategies [3–14]. An adaptive sliding mode controller based on the LFC model of photovoltaic energy storage systems has been designed in [3]. A machine learning-based emergency voltage stabilization model predictive control (MPC) has been proposed to implement acceleration strategies in real time for power systems in [4]. A multi-area IPS-LFC method under spurious data injection attacks has been investigated in [5]. In reference[6], the

authors have investigated the exponential rejection trouble of an LFC model of a multi-area IPS with input time lags. To rectify the objective function of the proportional-integral-derivative (PID) control parameters, a PID controller for the LFC of IPS has been proposed using an ant colony algorithm in [8]. In reference[9], the authors have proposed a new method Harris Hawk Optimizer (HHO) to solve the frequency constraint obstacle to effectively suppress wiring power exchange and frequency dynamic oscillations in a multi-area IPS. In reference[10], the authors have proposed a fuzzy PI/PID hybrid optimization controller based on differential evolution and pattern search to solve the LFC obstacle of IPS. In order to improve the frequency stability of the energy grid, the authors have proposed a different method for controlling the frequency of the load with three degrees of freedom in [11]. In order to integrate the power system with the effective contribution of renewable energy, a grid model for studying the LFC problem has been proposed in [12]. In reference[13], the authors have proposed an adaptive LFC technique for isolated and interconnected microgrids. The Jaya optimization method has been used for the area controller online.

With the rapid development of the social economy, people's requirements for power systems and power equipment are increasing. The structure and function are becoming more and more complex, and the degree of automation and intelligence of the power system is becoming higher and higher. Various power subsystems and an increasing number of smaller power systems are being integrated into the large power grid, forming an IPS that makes full use of energy in remote areas.

Due to the limitations of the natural environment, there are still many problems with IPS technologies. For example, wind and solar energy are stochastic and intermittent, resulting in a power system with stochastic and intermittent power output. Secondly, distributed power sources are difficult to control, costly, and have weak malfunction ride-through capability when connected to the main grid [15]. The IEEE P1547 protocol, published in 2001, explicitly requires that distributed power sources be immediately disconnected from the main grid when a malfunction occurs on the main grid [16]. This operation will cause power imbalances in transient processes within the grid system. In reference[17], an improved convolutional neural network-based malfunction diagnosis method for ship power systems has been proposed to support the normal operation of ships. In reference[18], a parameter-free active malfunction-tolerant control strategy for LFC has been proposed. The malfunction diagnosis consists of three parts, namely, malfunction de-

Manuscript received March 4, 2023; revised August 17, 2024. The research work was supported by the Fundamental Research Funds for the Liaoning Universities.

Ziming Wang is a postgraduate student of School of Electronic and Information Engineering, University of Science and Technology Liaoning, Anshan, 114051, China. (e-mail: 1094342407@qq.com).

Zhao Zhang is an associate professor of School of Computer Science and Software Engineering, University of Science and Technology Liaoning, Anshan, 114051, China. (corresponding author, e-mail: zhangzhao333@hotmail.com).

Hongyan Zhou is a doctoral student of School of Electronic and Information Engineering, University of Science and Technology Liaoning, Anshan, 114051, China. (e-mail: zhou321yan@163.com).

Xue-Bo Chen is a professor of School of Electronic and Information Engineering, University of Science and Technology Liaoning, Anshan, 114051, China. (e-mail: xuebochen@126.com).

tection, malfunction separation, and malfunction estimation [19]. A design scheme for distributed malfunction detection and isolation filters has been proposed in [20]. An observer-based malfunction isolation and detection method has been proposed in [19].

The malfunction estimation method over other malfunction diagnosis methods is that the malfunction signal can be recovered, and the malfunction information is more in-depth, including the complete waveform and amplitude of the malfunction source [21, 22]. The method in [23] allows rapid detection of engine malfunctions, estimate of thrust loss using the malfunction estimation method, and accurate location of the serial number of malfunctioning engines in a power system consisting of multiple engines.

Therefore, malfunction estimation can improve the safety and reliability of power systems by monitoring and analyzing real-time data of power systems, analyzing malfunctions more accurately, identifying and locating malfunctioning equipment or system components, and helping to respond to malfunctions more quickly, locating them more accurately, and repair them more effectively. However, most of the available research results rarely consider the distributed malfunction estimation. As a typical multi-agent systems (MAS), multi-area IPS can optimize the overall malfunction estimation performance by adding multi-agent communication. Researchers have proposed several malfunction estimation methods for MAS. In [24], the authors have proposed a distributed malfunction estimation method that designs unknown input observers for each agent independently and estimates the state and malfunction signals. In [25, 26], the authors have designed intermediate observers for linear/nonlinear systems, respectively. In [27], the sliding mode observer method has been used to estimate actuator malfunctions. To compute the parameter matrix of the observer, a feasible linear matrix inequality (LMI) solution has been needed [24, 28, 29]. The sequence of LMI along with the number of agents. As a result, the computational effort also increases the number of agents. In [30], the authors have used an LMI based on the Schur decomposition theorem to solve matrix parameters of the same dimension as a single system, and its computational effort has not been affected by the number of agents in the systems. Therefore, a set of intermediate observers has been designed for the control unit of IPS to estimate the status of IPS and the malfunction of actuators and sensors.

In summary, this paper investigates the difficulty of malfunction estimation in IPS. The main contributions and innovations of this paper include:

- 1) An intermediate variable observer is designed to estimate the malfunction signals of the IPS control unit, which overcomes the observer matching condition required by most observers.
- 2) Unlike most existing studies that have mostly considered only malfunction estimation for centralized systems. In this paper, the estimation accuracy of malfunction signals is improved by increasing the communication between IPS and collecting neighbor signals.
- 3) Compared with the traditional intermediate observer malfunction estimation method, this method adopts multi-agent topology and introduces output estimation

error feedback, including both distributed and centralized estimation errors, thus improves the estimation performance.

II. PROBLEM DESCRIPTION AND MODELING

For a directed graph $\mathcal{G}(\mathcal{V}, \mathcal{E}, \mathcal{A})$, $\mathcal{V} = [V_1, V_2, \dots, V_N]$ is a set of non-empty points, and V_i is the i th node, i is a positive integer; $\mathcal{E} = [(V_i, V_j) : V_i, V_j \in \mathcal{V}] \subset \mathcal{V} \times \mathcal{V}$ is the edge set of the topology; $\mathcal{A} = [a_{ij}] \in R^{N \times N}$ is the adjacency matrix of the graph \mathcal{G} , where $a_{ij} = 1$ when $V_i, V_j \in \mathcal{E}$, and $a_{ij} = 0$ when $V_i, V_j \notin \mathcal{E}$. V_j is a neighbor of V_i only if $V_i, V_j \in \mathcal{E}$. Matrix $\mathcal{L} = [l_{ij}] \in R^{N \times N}$ is the Laplacian matrix, which is defined as $\mathcal{L} = \mathcal{D} - \mathcal{A}$, where \mathcal{D} is the degree matrix, where $l_{ij} = \sum_{j=1, j \neq i}^N a_{ij}$, and $l_{ij} = -a_{ij}$, $i \neq j$. Undirected graphs are also a special kind of directed topology map.

A. Problem Formulation

For a large power system, it consists of many interlinked control areas. Fig. 1 shows a diagram of control area i . In LFC design, generators, turbines and powertrain units are typically modeled using three first-order transfer functions $\sum_{j=1, j \neq i}^N T_{ij} \Delta f_i$ and ΔP_{Li} are the area interface and the local load perturbation, respectively. After the load perturbation in the control area, the frequency in the control area changes transiently and the feedback takes into play to generate the corresponding rise or fall signals to each generator based on the participation factor (a_{ij}) for each generator, the generation needs to follow the load. In the steady working condition, the generators need to match the load, following which both the power and frequency deviation of the contact line are zero. An area control error (ACE) signal is generated through input frequency and contact line power deviations to achieve a balance between the connected control areas. This generates an ACE signal which is in turn used in the PI control, where ACE signal is defined as $\beta_i \Delta f_i(t) + \Delta P_{tie,i}(t)$. They mean a linear combination of variations of contact line power and frequency deviations.

The reference [31] has provided a simplified linear model of IPS, among which the diagram of the i th control area is shown in Fig. 1. Its kinetic is described as follows:

$$\begin{cases} \Delta \dot{f}_i(t) = \frac{1}{M_i} (\Delta P_{mi}(t) - D_i \Delta f_i(t) - \Delta P_{Li}(t) - \Delta P_{tie,i}(t)), \\ \Delta \dot{P}_{tie,i}(t) = 2\pi \sum_{j=1, j \neq i}^N T_{ij} (\Delta f_i(t) - \Delta f_j(t)), \\ \Delta \dot{P}_{mi}(t) = \frac{1}{T_{ti}} (\Delta P_{gi}(t) - \Delta P_{mi}(t)), \\ \Delta \dot{P}_{gi}(t) = \frac{1}{T_{gi}} (\Delta P_{ci}(t) - \frac{1}{R_i} \Delta f_i(t) - \Delta P_{gi}(t)). \end{cases} \quad (1)$$

In the actual control work, it is also necessary to collect the variation of the generator's mechanical power and the governor's movement. Therefore, we selected ACE_i as y_{i1} , the mechanical power variation of the generator as y_{i2} , and the movement of the governor as y_{i3} , and

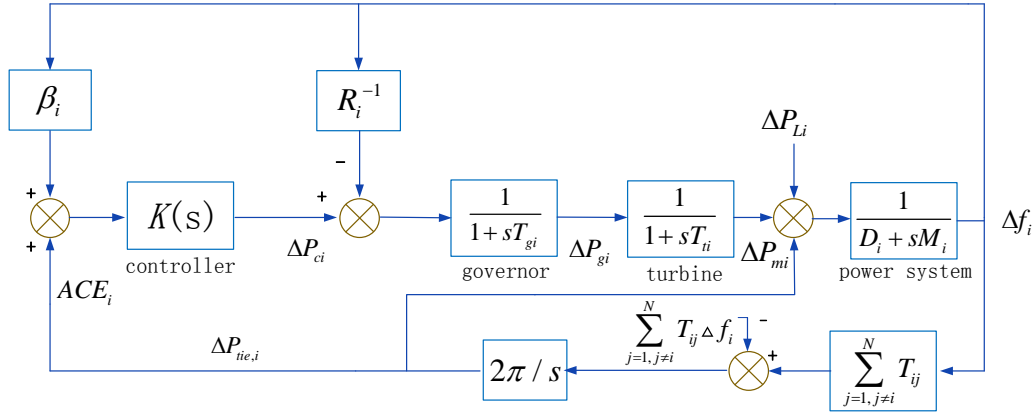


Fig. 1: Interconnected power system model.

$y_i = [y_{i1}, y_{i2}, y_{i3}]^T$. The relevant system parameters and variables are defined in Table I.

Further, the dynamics equation (1) of the power system is described as:

$$\begin{cases} \dot{x}_i(t) = A_i x_i(t) + B_i u_i(t) + H_{0i} w_i(t), \\ y_i(t) = C_i x_i(t), \end{cases} \quad (2)$$

here $x_i(t) = [\Delta f_i(t), \Delta P_{tie,i}(t), \Delta P_{mi}(t), \Delta P_{gi}(t)]^T$, $w_i(t) = [\Delta P_{Li}(t), \sum_{j=1, j \neq i}^N T_{ij} \Delta f_i(t)]^T$, the matrices A_i , B_i , C_i , and H_{0i} are shown in Formula (3), and $u_i(t) = \Delta P_{ci}(t)$, $y_i(t) \in R^{n_y}$ for measurement output. They belong to the i th area.

$$A_i = \begin{bmatrix} -\frac{D_i}{M_i} & \frac{1}{M_i} & \frac{1}{L_i} & 0 \\ 2\pi \sum_{j=1, j \neq i}^N T_{ij} & 0 & 0 & 0 \\ 0 & 0 & -\frac{1}{T_{ti}} & \frac{1}{T_{gi}} \\ \frac{1}{R_i T_{gi}} & 0 & 0 & -\frac{1}{T_{gi}} \end{bmatrix},$$

$$B_i = \begin{bmatrix} 0 & 0 & 0 & \frac{1}{T_{gi}} \end{bmatrix}^T,$$

$$C_i = \begin{bmatrix} \beta_i & 1 & 0 & 0 \\ 0 & 0 & 1 & 0 \\ 0 & 0 & 0 & 1 \end{bmatrix}, H_{0i} = \begin{bmatrix} -\frac{1}{M_i} & 0 & 0 & 0 \\ 0 & -2\pi & 0 & 0 \end{bmatrix}^T. \quad (3)$$

Considering the malfunctions of the sensor and actuator, the power system with the following area i dynamics:

$$\dot{x}_i(t) = A_i x_i(t) + B_i u_i(t) + H_{1i} g_{1i}(t) + H_{0i} w_i(t), \quad (4)$$

TABLE I: Definition of power system signals.

Symbol	Definition
Δf_i	Frequency deviation
ΔP_{mi}	Mechanical power variation of generator
ΔP_{gi}	Motion of the governor
ΔP_{Li}	Load disturbance
$\Delta P_{tie,i}$	Contact line power deviation
ΔP_{ci}	Secondary frequency modulation action
M_i	Equivalent inertia coefficient
T_{gi}	Governor time constant
T_{ij}	Synchronization coefficient of contact line
T_{ti}	Prime mover time constant
R_i	Droop characteristic
D_i	Equivalent damping coefficient
β_i	Frequency deviation factor

$$y_i(t) = C_i x_i(t) + H_{2i} g_{2i}(t), \quad (5)$$

where $g_{1i}(t) \in R^{n_{g1}}$ are the vector of actuator malfunction and $g_{2i}(t) \in R^{n_{g2}}$ are the vector of sensor malfunction. H_{1i} , H_{2i} are some matrices with corresponding dimensions. If $g_{1i}(t)$ and $g_{2i}(t)$ are differentiable. This assumption is common in many malfunction studies literature, such as [24, 27–29, 32–34].

The principle purpose of this paper is: using the output of each region and the output of other regions in the network, design a malfunction observer to achieve the estimation of states $x_i(t)$, malfunctions $g_{1i}(t)$ and $g_{2i}(t)$.

III. MAJOR RESEARCH RESULTS

A. State variable Transformation

Make $\bar{x}_i^T(t) = [x_i^T(t), g_{2i}^T(t)]^T$, subsequently the system dynamic (4) and (5) are reconfigured as

$$K_0 \dot{\bar{x}}_i(t) = A_{1i} \bar{x}_i(t) + \bar{B}_i u_i(t) + \bar{H}_{1i} g_{1i}(t) + \bar{H}_{0i} d_i(t) + T_1 H_{2i} g_{2i}(t), \quad (6)$$

$$y_i(t) = C_{1i} \bar{x}_i(t) = C_{0i} \bar{x}_i(t) + H_{2i} g_{2i}(t), \quad (7)$$

where

$$K_0 = \begin{bmatrix} I_n & 0 \\ 0 & 0_{n_y \times n_{fs}} \end{bmatrix}, A_{1i} = \begin{bmatrix} A_i & 0 \\ 0 & -D_{si} \end{bmatrix},$$

$$\bar{B}_i = \begin{bmatrix} B_i \\ 0_{n_y \times n_u} \end{bmatrix}, \bar{H}_{1i} = \begin{bmatrix} H_{1i} \\ 0_{n_y \times n_{g1}} \end{bmatrix},$$

$$\bar{H}_{0i} = \begin{bmatrix} H_{0i} \\ 0_{n_y \times n_w} \end{bmatrix}, T_1 = \begin{bmatrix} 0_{n \times n_y} \\ I_{n_y} \end{bmatrix},$$

$$T_0 = [I_n \quad 0_{n \times n_{fs}}], C_{1i} = [C_i \quad H_{2i}],$$

$$C_{0i} = [C_i \quad 0_{n_y \times n_{fs}}].$$

From (7), we have that $H_{2i} g_{2i}(t) = y_i(t) - C_{0i} \bar{x}_i(t)$. Substituting it into (6), we possess

$$K_0 \dot{\bar{x}}_i(t) = (A_{1i} - T_1 C_{0i}) \bar{x}_i(t) + \bar{B}_i u_i(t) + \bar{H}_{1i} g_{1i}(t) + \bar{H}_{0i} w_i(t) + T_1 y_i(t). \quad (8)$$

Make $E = \begin{bmatrix} 0_{n \times n_y} \\ E_0 \end{bmatrix}$, where E_0 is a nonsingular matrix and $E_0 \in R^{n_y \times n_y}$. Add $EC_{1i} \bar{x}_i(t)$ to either side of (8),

subsequently

$$K_{1i} \ddot{\bar{x}}_i(t) = (A_{1i} - T_1 C_{0i}) \bar{x}_i(t) + \bar{B}_i u_i(t) + \bar{H}_{1i} g_{1i}(t) + \bar{H}_{0i} w_i(t) + T_1 y_i(t) + EC_{1i} \dot{\bar{x}}_i(t),$$

where $K_{1i} = K_0 + EC_{1i} = \begin{bmatrix} I_n & 0 \\ E_0 C_i & E_0 H_{2i} \end{bmatrix}$. Let $K_{1i}^- = \begin{bmatrix} I_n & 0 \\ -H_{2i}^- C_i & H_{2i}^- E_0^{-1} \end{bmatrix}$, where H_{2i}^- is a left inverse matrix of H_{2i} , and $H_{2i}^- H_{2i} = I$. Thus, $K_{1i}^- K_{1i} = I$.

Then the following system is obtained by us:

$$\dot{\bar{x}}_i(t) = A_{2i} \bar{x}_i(t) + \bar{B}_{1i} u_i(t) + H_{3i} g_{1i}(t) + H_{4i} w_i(t) + T_2 y_i(t) + E_{2i} C_{1i} \dot{\bar{x}}_i(t), \quad (9)$$

where $A_{2i} = K_{1i}^- (A_{1i} - T_1 C_0)$, $\bar{B}_{1i} = K_{1i}^- \bar{B}_i$, $H_{3i} = K_{1i}^- \bar{H}_{1i}$, $T_2 = K_{1i}^- T_1$, $H_{4i} = K_{1i}^- \bar{H}_{0i}$, $E_{2i} = K_{1i}^- E$.

Combining (7) and (9), we get

$$\dot{\bar{x}}_i(t) = A_{2i} \bar{x}_i(t) + \bar{B}_{1i} u_i(t) + H_{3i} g_{1i}(t) + H_{wi} w_i(t) + T_2 y_i(t) + E_{2i} \dot{y}_i(t), \quad (10)$$

where $\bar{w}_i(t) = [w_i^T(t), \dot{g}_{1i}^T(t)]^T$, $H_{wi} = [H_{4i}, 0_{(n+n_{g2}) \times n_{g1}}]$.

B. Design of the State Observer

Next, an intermediate variable $\zeta_i(t)$ will be chosen to design the observer to realize the estimation of $\bar{x}_i(t)$ and $g_{1i}(t)$ for each area i . It is defined as [26]:

$$\zeta_i(t) = g_{1i}(t) - \varpi_i(\bar{x}_i(t) - E_{2i} y_i(t)), \quad (11)$$

where ϖ_i will be defined in next subsection. From (10), we can get that

$$\dot{\zeta}_i(t) = \dot{g}_{1i}(t) - \varpi_i[A_{2i} \bar{x}_i(t) + \bar{B}_{1i} u_i(t) + H_{3i} g_{1i}(t) + T_2 y_i(t) + H_{wi} w_i(t)]. \quad (12)$$

From (7), (10), and (12), the region i 's observer is constructed as:

$$\dot{\hat{z}}_i(t) = A_{2i} \hat{z}_i(t) + \bar{B}_{1i} u_i(t) + H_{3i} \hat{g}_{1i}(t) + (A_{2i} E_{2i} + T_2 y_i(t)) + \rho_1 L_{1i} \xi_{1i}(t) + \rho_2 L_{2i} \xi_{2i}(t), \quad (13)$$

$$\dot{\hat{\zeta}}_i(t) = -\varpi_i H_{3i} \hat{\zeta}_i(t) + \rho_1 L_{3i} \xi_{1i}(t) + \rho_2 L_{4i} \xi_{2i}(t) - \varpi_i [A_{2i} \hat{x}_i(t) + \bar{B}_{1i} u_i(t) + H_{3i} \varpi_i \hat{z}_i(t) + T_2 y_i(t)], \quad (14)$$

$$\hat{\bar{x}}_i(t) = \hat{z}_i(t) + E_{2i} y_i(t), \quad (15)$$

$$\hat{g}_{1i}(t) = \hat{\zeta}_i(t) + \varpi_i(\hat{\bar{x}}_i(t) - E_{2i} y_i(t)), \quad (16)$$

$$\hat{y}_i(t) = C_{1i} \hat{\bar{x}}_i(t), \quad (17)$$

where $\hat{\bar{x}}_i(t)$ is the estimation of $\bar{x}_i(t)$. $\hat{\zeta}_i(t)$, $\hat{g}_{1i}(t)$, $\hat{z}_i(t) \in R^{n+n_{g2}}$, $\hat{\zeta}_i(t) \in R^{n_{g1}}$ and $\hat{y}_i(t)$ are also like $\bar{x}_i(t)$. The centralized/distributed output estimation error ξ_{1i} / ξ_{2i} are defined as $y_i(t) - \hat{y}_i(t)$ and $\sum_{j=1}^N a_{ij} [(y_j(t) - \hat{y}_j(t)) - (y_j(t) - \hat{y}_j(t))]$, respectively. $L_{1i} \in R^{(n+n_{g2}) \times n_y}$, $L_{2i} \in R^{(n+n_{g2}) \times n_y}$, $L_{3i} \in R^{n_{g1} \times n_y}$, $L_{4i} \in R^{n_{g1} \times n_y}$ are the parameter matrices we will design later. The weighted indexes ρ_1 and ρ_2 are nonnegative constants and satisfy $\rho_1 + \rho_2 = 1$ and $0 \leq \rho_1 \leq 1$, $0 \leq \rho_2 \leq 1$.

C. Estimation Error Dynamic Construction

In this article, we refer to [32] and [34] to define ϖ_i .

$$\varpi_i = 3H_{3i}^T. \quad (18)$$

Make $\tilde{x}_i(t) = \bar{x}_i(t) - \hat{\bar{x}}_i(t)$. According to (10), (13) and (15), it can be found that

$$\dot{\tilde{x}}_i(t) = (A_{2i} - \rho_1 L_{1i} C_{1i}) \tilde{x}_i(t) + H_{3i} \tilde{g}_{1i} + H_{wi} w_i(t) - \rho_2 L_{2i} \xi_{2i}(t), \quad (19)$$

in the formula $\tilde{g}_{1i}(t) = g_{1i}(t) - \hat{g}_{1i}(t)$.

Let $\tilde{\zeta}_i(t) = \zeta_i(t) - \hat{\zeta}_i(t)$. From (12) and (14), we have that

$$\begin{aligned} \dot{\tilde{\zeta}}_i(t) &= \dot{\zeta}_i(t) - \dot{\hat{\zeta}}_i(t) \\ &= \dot{g}_{1i}(t) - \varpi_i A_{2i} \tilde{x}_i(t) - \varpi_i H_{3i} g_{1i}(t) - \varpi_i H_{wi} w_i(t) \\ &\quad + \varpi_i H_{3i} - \hat{\zeta}_i(t) + \varpi_i H_{3i} \varpi_i \hat{z}_i(t) - \rho_1 L_{3i} \xi_{1i}(t) \\ &\quad - \rho_2 L_{4i} \xi_{2i}(t) \\ &= \dot{g}_{1i}(t) - \varpi_i A_{2i} \tilde{x}_i(t) - \varpi_i H_{wi} w_i(t) - \rho_1 L_{3i} \xi_{1i}(t) \\ &\quad - \rho_2 L_{4i} \xi_{2i}(t) - \varpi_i H_{3i} [g_{1i}(t) - \hat{\zeta}_i(t) - \varpi_i \hat{z}_i(t)]. \end{aligned}$$

From (11) and (15), it can be seen $g_{1i}(t) = \zeta_i(t) + \varpi_i(\bar{x}_i(t) - E_{2i} y_i(t))$ and $\hat{z}_i(t) = \hat{\zeta}_i(t) - E_{2i} y_i(t)$, plug them into $\tilde{\zeta}_i(t)$, we get

$$\begin{aligned} \dot{\tilde{\zeta}}_i(t) &= \dot{g}_{1i}(t) - \varpi_i A_{2i} \tilde{x}_i(t) - \varpi_i H_{wi} w_i(t) - \rho_1 L_{3i} \xi_{1i}(t) \\ &\quad - \rho_2 L_{4i} \xi_{2i}(t) - \varpi_i H_{3i} [\tilde{\zeta}_i(t) + \varpi_i \tilde{x}_i(t)] \\ &= \dot{g}_{1i}(t) - (\varpi_i A_{2i} + \varpi_i H_{3i} \varpi_i) \tilde{x}_i(t) - \varpi_i H_{wi} w_i(t) \\ &\quad - \rho_1 L_{3i} \xi_{1i}(t) - \rho_2 L_{4i} \xi_{2i}(t) - \varpi_i H_{3i} \tilde{\zeta}_i(t). \end{aligned}$$

From (7) and (17), $\xi_{1i}(t) = C_{1i} \tilde{x}_i$, merging (18) and $\xi_{2i}(t)$, it can be seen that

$$\begin{aligned} \dot{\tilde{\zeta}}_i(t) &= -3H_{3i}^T H_{3i} \tilde{\zeta}_i(t) + D_{wi} w_i(t) - \rho_2 L_{4i} \xi_{2i}(t) \\ &\quad - (3H_{3i}^T (A_{2i} + 3H_{3i} H_{3i}^T) + \rho_1 L_{3i} C_{1i}) \tilde{x}_i(t), \quad (20) \end{aligned}$$

where $J_{wi} = -3H_{3i}^T H_{wi} + [0_{n_{g1} \times n_w} \ I_{n_{g1}}]$ and $\bar{w}_i(t) = [w_i^T(t) \ \dot{g}_{1i}^T(t)]$. From (11), (16), and (18), we have that

$$\tilde{g}_{1i} = \tilde{\zeta}_i + \varpi_i \tilde{x}_i = \tilde{\zeta}_i + 3H_{3i}^T \tilde{x}_i.$$

Thus, (19) can be rewritten as

$$\begin{aligned} \dot{\tilde{x}}_i(t) &= (A_{2i} + 3H_{3i} H_{3i}^T - \rho_1 L_{1i} C_{1i}) \tilde{x}_i(t) + H_{3i} \tilde{\zeta}_i \\ &\quad + H_{wi} w_i(t) - \rho_2 L_{2i} \xi_{2i}(t), \quad (21) \end{aligned}$$

Let $e_i(t) = [\tilde{x}_i^T(t), \tilde{\zeta}_i^T(t)]^T$, merge (20) and (21), subsequently the dynamics can be obtained as:

$$\dot{e}_i(t) = (A_{3i} - \rho_1 \bar{L}_{1i} C_{3i}) e_i(t) + \bar{H}_{wi} w_i(t) - \rho_2 \bar{L}_{2i} \xi_{2i}(t), \quad (22)$$

where

$$\begin{aligned} A_{3i} &= \begin{bmatrix} A_{2i} + 3H_{3i} H_{3i}^T & H_{3i} \\ -3H_{3i}^T (A_{2i} + 3H_{3i} H_{3i}^T) & -3H_{3i}^T H_{3i} \end{bmatrix}, \\ \bar{L}_{1i} &= \begin{bmatrix} L_{1i} \\ L_{3i} \end{bmatrix}, \bar{L}_{2i} = \begin{bmatrix} L_{2i} \\ L_{4i} \end{bmatrix}, \\ C_{3i} &= [C_{1i} \ 0_{n_y \times n_{g1}}], \bar{H}_{wi} = \begin{bmatrix} H_{wi} \\ J_{wi} \end{bmatrix}. \end{aligned}$$

In (22), we have

$$\begin{aligned} A_{3i} - \rho_1 \bar{L}_{1i} C_{3i} &= \\ &= \begin{bmatrix} A_{2i} + 3H_{3i} H_{3i}^T - \rho_1 L_{1i} C_{1i} & H_{3i} \\ -3H_{3i}^T (A_{2i} + 3H_{3i} H_{3i}^T) - \rho_1 L_{3i} C_{1i} & -3H_{3i}^T H_{3i} \end{bmatrix}. \end{aligned}$$

It can be found that the (2, 2) element of the matrix $A_{3i} - \rho_1 \bar{L}_{1i} C_{3i}$ is $-\varpi_i H_{3i}$. Note that $H_{3i} = K_{1i}^{-1} \bar{H}_{1i} = \begin{bmatrix} H_{1i} \\ -H_{2i}^{-1} C_i H_{1i} \end{bmatrix}$. From (18), the parameter ϖ_i is selected as $\varpi_i = 3H_{3i}^T$. Thus, we have that $-\varpi_i H_{3i} = -3H_{3i}^T H_{3i} < 0$, which can ensure that all eigenvalues of $A_{3i} - \rho_1 \bar{L}_{1i} C_{3i}$ are with negative real part. Therefore, the global error dynamic can be obtained as:

$$\dot{e}(t) = I_N \otimes (A_{3i} - \rho_1 \bar{L}_{1i} C_{3i}) e(t) - \mathcal{L} \otimes (\rho_2 \bar{L}_{2i} C_{3i}) e(t) + I_N \otimes \bar{H}_{wi} w(t), \quad (23)$$

in the formula

$$e(t) = [e_1^T(t), e_2^T(t), \dots, e_N^T(t)]^T, \\ w(t) = [w_1^T(t), w_2^T(t), \dots, w_N^T(t)]^T.$$

D. Robustness Analysis

Theorem 1. For given constants ρ_1 , ρ_2 , and γ , $\dot{e}(t)$ is asymptotically stable under the H_∞ index γ . If there is a symmetric positive definite matrix $P \in R^{(n+n_{g2}+n_{g1}) \times (n+n_{g2}+n_{g1})}$, matrix $Q \in R^{(n+n_{g2}+n_{g1}) \times n_y}$, positive constants κ , make the LMI inequality established:

$$\begin{bmatrix} \bar{\Phi}_i - (\lambda_{\min} \rho_2 \kappa C_{3i}^T C_{3i}) & P_i \bar{H}_{wi} \\ * & -\gamma^2 I \end{bmatrix} < 0, \quad (24)$$

in the formula, λ_{\min} is the smallest eigenvalue of all eigenvalues of $\mathcal{L}^T + \mathcal{L}$, $\bar{\Phi}_i = (P_i A_{3i} - \rho_1 Q_{1i} C_{3i}) + (P_i A_{3i} - \rho_1 Q_{1i} C_{3i})^T + I$, $\bar{L}_{1i} = P_i^{-1} Q_i$, $\bar{L}_{2i} = \kappa P_i^{-1} C_{3i}^T$

Proof: The Lyapunov function is selected to be of the this form:

$$V = e^T(t) (I_N \otimes P_i) e(t).$$

When $w(t) = 0$, along (23), the differential of $V(t)$ is

$$\dot{V} = e^T(t) [I_N \otimes (P_i A_{3i} - \rho_1 Q_{1i} C_{3i}) + I_N \otimes (P_i A_{3i} - \rho_1 Q_{1i} C_{3i})^T] e(t) - e^T(t) [(\mathcal{L}^T + \mathcal{L}) \otimes (\rho_2 \kappa C_{3i}^T C_{3i})] e(t),$$

where $Q_{1i} = P_i \bar{L}_{1i}$, $\bar{L}_{2i} = \kappa P_i^{-1} C_{3i}^T$.

Make $\bar{\Phi}_i = (P_i A_{3i} - \rho_1 Q_{1i} C_{3i}) + (P_i A_{3i} - \rho_1 Q_{1i} C_{3i})^T$. Obviously, if

$$I_N \otimes \bar{\Phi}_i - (\mathcal{L}^T + \mathcal{L}) \otimes (\rho_2 \kappa C_{3i}^T C_{3i}) < 0, \quad (25)$$

then $\dot{V}(t) < 0$, which means $\dot{e}(t)$ is stable when $w(t) = 0$.

Because there is a symmetric matrix $\mathcal{L}^T + \mathcal{L}$, Schur factorization theory assumes that a matrix M satisfies:

$$M^T (\mathcal{L}^T + \mathcal{L}) M = \Lambda, \quad (26)$$

in the formula Λ is the diagonal matrix of i th eigenvalues of $\mathcal{L}^T + \mathcal{L}$, and $M^T M = I$.

To the left of formula (25) multiplied by $M^T \otimes I$, and on the right side of formula (25) multiplied by $M \otimes I$.

The inequality is transformed by:

$$I_N \otimes \bar{\Phi}_i - \Lambda \otimes (\rho_2 \kappa C_{3i}^T C_{3i}) < 0. \quad (27)$$

Because of the properties of diagonal matrices, so that (27) holds only if when $i = 1, 2, \dots, N$, then there are inequalities:

$$\bar{\Phi}_i - \lambda_i \rho_2 \kappa C_{3i}^T C_{3i} < 0. \quad (28)$$

Note that $\rho_2 \geq 0$ and $\kappa > 0$, we have that $\rho_2 \kappa C_{3i}^T C_{3i} \geq 0$. Obviously

$$\bar{\Phi}_i - \lambda_i \rho_2 \kappa C_{3i}^T C_{3i} \leq \bar{\Phi}_i - \lambda_{\min} \rho_2 \kappa C_{3i}^T C_{3i}. \quad (29)$$

So, if the LMI holds:

$$\bar{\Phi}_i - \lambda_{\min} \rho_2 \kappa C_{3i}^T C_{3i} < 0, \quad (30)$$

it can be found that LMI (28) is satisfied.

If (24) is feasible, we have that $\dot{V}(t) < 0$. So, if (24) is possible, (23) is asymptotically stable when $w(t) = 0$. Next, make us to consider when $w(t) \neq 0$. The $V(t)$'s differential along (23) is

$$\dot{V}(t) = e^T(t) [I_N \otimes (P_i A_{3i} - \rho_1 Q_{1i} C_{3i}) + I_N \otimes (P_i A_{3i} - \rho_1 Q_{1i} C_{3i})^T] e(t) - e^T(t) [(\mathcal{L}^T + \mathcal{L}) \otimes (\rho_2 \kappa C_{3i}^T C_{3i})] e(t) + 2e^T(t) (I_N \otimes (P_i \bar{B}_{wi})) w(t).$$

It's like when $w(t) = 0$, take (25) and put it into (31), so

$$\dot{V}(t) \leq e^T(t) [I_N \otimes \bar{\Phi}_i - (\mathcal{L}^T + \mathcal{L}) \otimes (\rho_2 \kappa C_{3i}^T C_{3i})] e(t) + 2e^T(t) (I_N \otimes (P_i \bar{H}_{wi})) w(t). \quad (31)$$

Let

$$\mathcal{J}(t) = \dot{V}(t) + e^T(t) e(t) - \gamma^2 w^T(t) w(t). \quad (32)$$

Merge (31) and (32), it becomes that

$$\mathcal{J}(t) \leq \begin{bmatrix} e(t) \\ w(t) \end{bmatrix}^T \begin{bmatrix} \tilde{\mathcal{L}} & I_N \otimes P_i \bar{H}_{wi} \\ * & -\gamma^2 I_N \otimes I_{n_w+n_{g1}} \end{bmatrix} \begin{bmatrix} e(t) \\ w(t) \end{bmatrix}, \quad (33)$$

where $\tilde{\mathcal{L}} = I_N \otimes \bar{\Phi}_i - (\mathcal{L}^T + \mathcal{L}) \otimes (\rho_2 \kappa C_{3i}^T C_{3i})$, here $\bar{\Phi}_i = \bar{\Phi}_i + I$. If this inequality holds:

$$\begin{bmatrix} \tilde{\mathcal{L}} & I_N \otimes P_i \bar{H}_{wi} \\ * & -\gamma^2 I_N \otimes I_{n_w+n_{g1}} \end{bmatrix} < 0, \quad (34)$$

so $\mathcal{J}(t) < 0$. Base on the zero initial condition, we have:

$$V(t) + \int_0^t [e^T(s) e(s) - \gamma^2 w^T(s) w(s)] ds < 0. \quad (35)$$

Since $V(t) = e^T(t) (I_N \otimes P_i) e(t)$ and P_i are positive definite matrixs, (35) means

$$\int_0^t [e^T(s) e(s)] ds < \int_0^t [\gamma^2 w^T(s) w(s)] ds. \quad (36)$$

In short, if (34) can derive (36). Premultiplying $\begin{bmatrix} M^T \otimes I_{n+n_{fa}+n_{fs}} & 0 \\ 0 & M^T \otimes I_{n_w+n_{fa}} \end{bmatrix}$ and postmultiplying $\begin{bmatrix} M \otimes I_{n+n_{fa}+n_{fs}} & 0 \\ 0 & M \otimes I_{n_w+n_{fa}} \end{bmatrix}$ in (34), we have

$$\begin{bmatrix} I_N \otimes \bar{\Phi}_i - \Lambda (\rho_2 \kappa C_{3i}^T C_{3i}) & I_N \otimes (P_i \bar{B}_{wi}) \\ 0 & -\gamma^2 I_N \otimes I_{n_w+n_{fa}} \end{bmatrix} < 0. \quad (37)$$

Thus, (37) holds only if when $i = 1, 2, \dots, N$,

$$\begin{bmatrix} \bar{\Phi}_i - (\lambda_{\min} \rho_2 \kappa C_{3i}^T C_{3i}) & P_i \bar{H}_{wi} \\ * & -\gamma^2 I \end{bmatrix} < 0. \quad (38)$$

Similar to the case when $w(t) = 0$, if (24) is reasonable, it can be found that (38) holds, which means (36) is tenable, and $\dot{e}(t)$ is asymptotically stable with the H_∞ performance index γ .

The stability of the system is proved. ■

IV. SIMULATION EXAMPLE

In this section, through an example of simulation verify the production of the proposed method.

Consider a three-area IPS. Its system topological graph is shown in Fig. 2. The numerical selection of model parameters [31] is shown in Table II, where the coefficient of contact line is, $T_{12} = 0.2(pu)/Hz$, $T_{13} = 0.25(pu)/Hz$, $T_{23} = 0.12(pu)/Hz$.

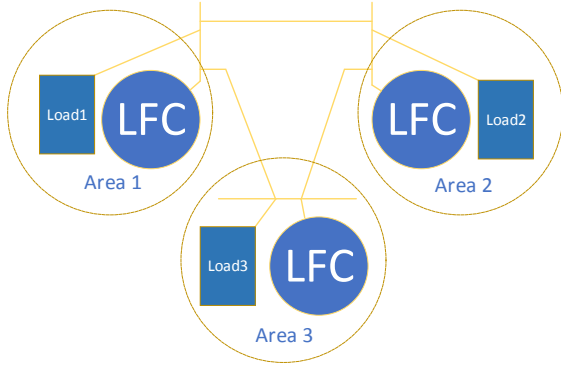


Fig. 2: Three-area interconnected power systems topological graph.

TABLE II: Simulation parameters of power system.

Parameters Setting	Area1	Area2	Area3
D	0.015	0.016	0.015
M	0.1667	0.2017	0.1247
R	3.00	2.73	2.82
β	0.3483	0.3827	0.3692
T_g	0.08	0.06	0.07
T_i	0.40	0.44	0.30
ρ_1	0.2	0.2	0.2
ρ_2	0.8	0.8	0.8

The topological correlation matrix is as follows:

$$\mathcal{A} = \begin{bmatrix} 0 & 1 & 1 \\ 1 & 0 & 1 \\ 1 & 1 & 0 \end{bmatrix}, \mathcal{L} = \begin{bmatrix} 1 & -1 & -1 \\ -1 & 1 & -1 \\ -1 & -1 & 1 \end{bmatrix}. \quad (39)$$

The malfunction coefficient matrices are selected as: $H_{1i} = [1, 1, 1, 1]^T$, $H_{2i} = [1, -2, 1]^T$, and assume that area 1 and area 2 have actuator malfunctions, area 2 and area 3 have sensor malfunctions. The effect of the simulation is shown in Fig. 3-8. It can be found that the observer can estimate all malfunctions simultaneously with relative accuracy.

V. CONCLUSIONS

In this paper, the state-space model of the control unit of the three-area IPS is developed, and an intermediate observer for state and malfunction estimation in a multi-agent network is designed. Collects adjacent signals to help estimate malfunction signals by increasing communication between multiple areas. Also, output feedback is introduced to enhance the estimation accuracy of centralized and distributed estimation malfunctions. Based on the performance of H_∞ , the robustness of the proposed method is improved by solving the gain matrix of the observer and transforming the problem of solving the gain matrix into a solvable problem of LMI. Finally, the effectiveness of the proposed

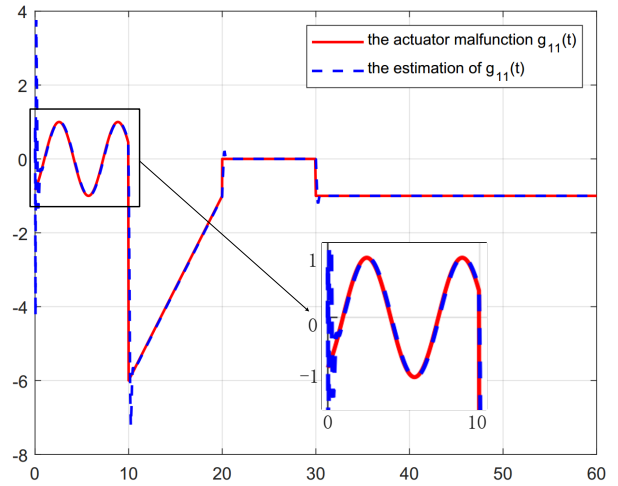


Fig. 3: Actuator malfunction in area 1, and the estimations of it.

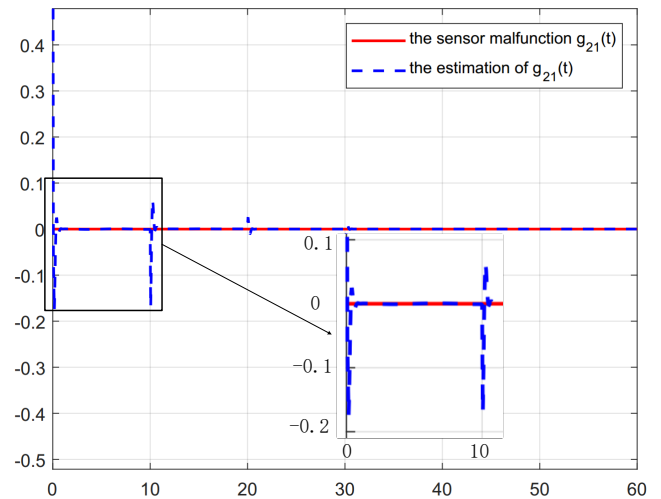


Fig. 4: Sensor malfunction in area 1, and the estimations of it.

method is verified by simulation experiments. In the future, active malfunction-tolerant control of MAS will be further investigated.

REFERENCES

- [1] J. Li, T. Hou, G. Mu, G. Yan, and C. Li, "Optimal control strategy for energy storage considering wind farm scheduling plan and modulation frequency limitation under electricity market environment," *Trans. China Electrotech. Soc.*, vol. 36, no. 9, pp. 1791–1804, 2021.
- [2] H. Rezk, M. A. Mohamed, A. Z. Diab, and N. Kanagaraj, "Load frequency control of multi-interconnected renewable energy plants using multi-verse optimizer," *Comput. Syst. Sci. Eng.*, vol. 37, no. 2, pp. 219–231, 2021.
- [3] Z. Wang and Y. Liu, "Adaptive terminal sliding mode based load frequency control for multi-area interconnected power systems with pv and energy storage," *IEEE Access*, vol. 9, pp. 120 185–120 192, 2021.
- [4] R. R. Hossain and R. Kumar, "Machine learning accelerated real-time model predictive control for power systems," *IEEE/CAA Journal of Automatica Sinica*, vol. 10, no. 4, pp. 916–930, 2023.

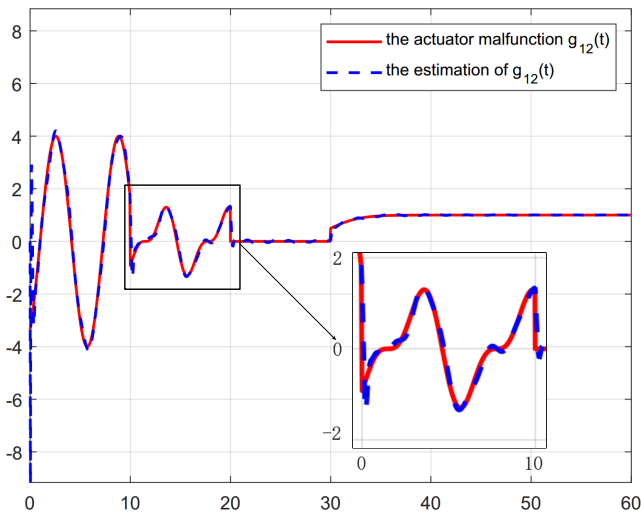


Fig. 5: Actuator malfunction in area 2, and the estimations of it.

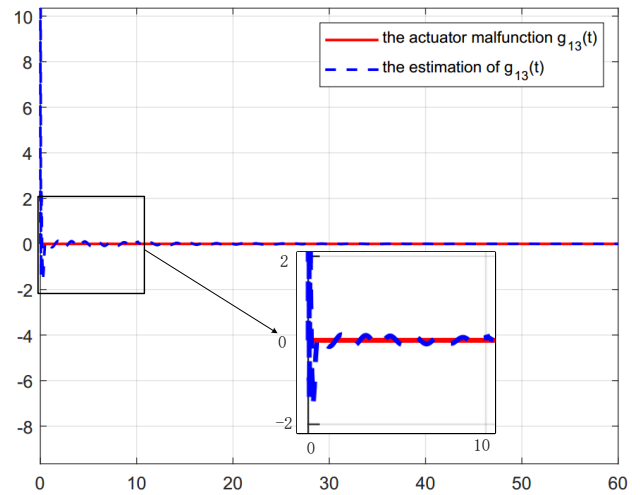


Fig. 7: Actuator malfunction in area 3, and the estimations of it.

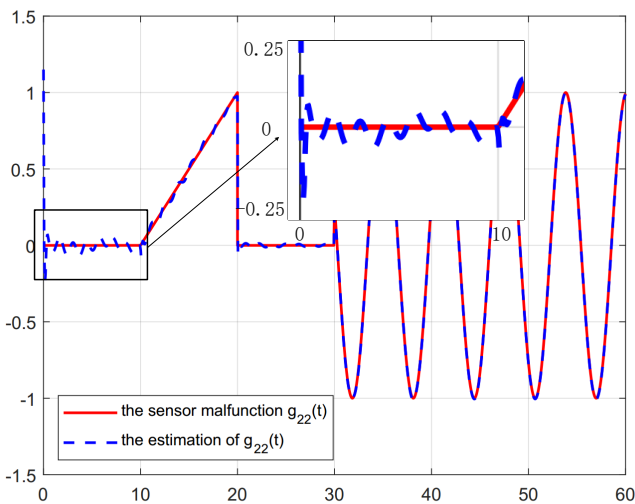


Fig. 6: Sensor malfunction in area 2, and the estimations of it.

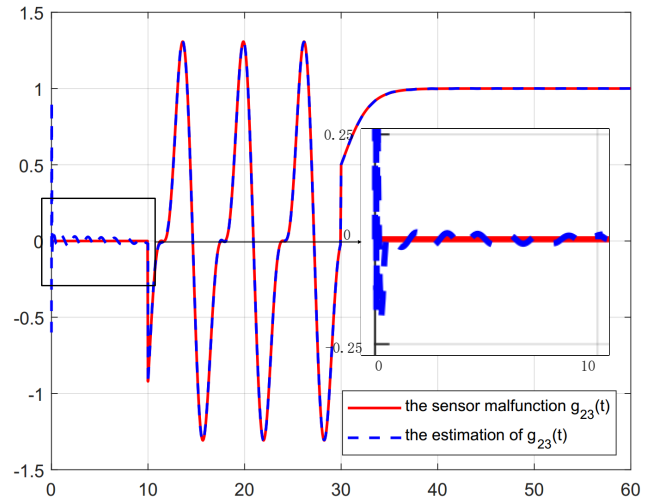


Fig. 8: Sensor malfunction in area 3, and the estimations of it.

- [5] T. Weng, Y. Xie, G. Chen, Q. Han, Y. Tian, L. Feng, and Y. Pei, "Load frequency control under false data inject attacks based on multi-agent system method in multi-area power systems," *International Journal of Distributed Sensor Networks*, vol. 18, no. 4, p. 15501329221090469, 2022.
- [6] D. T. Phuong, T. N. Pham, and L. V. Hien, "Exponential stabilization via tracking convergent rate in load frequency control of multi-area power systems with diverse communication delays," *International Journal of Dynamics and Control*, vol. 10, no. 1, pp. 107–121, 2022.
- [7] C. N. S. Kalyan and C. V. Suresh, "Higher order degree of freedom controller for load frequency control of multi area interconnected power system with time delays," *Global Transitions Proceedings*, vol. 3, no. 1, pp. 332–337, 2022.
- [8] K. Jagatheesan, B. Anand, N. Dey, A. S. Ashour, and V. E. Balas, "Proportional-integral-derivative (pid) controller equipped lfc of multi-area interconnected power system," in *V International Conference Industrial Engineering and Environmental Protection*, pp. 15–16, 2015.
- [9] A. D. Falehi, "Optimal design of fuzzy-agc based on pso & rcga to improve dynamic stability of interconnected multi area power systems," *International Journal of Automation and Computing*, vol. 17, no. 4, pp. 599–609, 2020.
- [10] R. K. Sahu, S. Panda, and N. K. Yegireddy, "A novel hybrid deps optimized fuzzy pi/pid controller for load frequency control of multi-area interconnected power systems," *Journal of Process Control*, vol. 24, no. 10, pp. 1596–1608, 2014.
- [11] E. M. Ahmed, E. A. Mohamed, A. Selim, M. Aly, A. Alsadi, W. Alhosaini, H. Alnuman, and H. A. Ramadan, "Improving load frequency control performance in interconnected power systems with a new optimal high degree of freedom cascaded fopid-tidf controller," *Ain Shams Engineering Journal*, vol. 14, no. 10, p. 102207, 2023.
- [12] M. A. Sobhy, A. Y. Abdelaziz, H. M. Hasanien, and M. Ezzat, "Marine predators algorithm for load frequency control of modern interconnected power systems including renewable energy sources and energy storage units," *Ain Shams Engineering Journal*, vol. 12, no. 4, pp. 3843–3857, 2021.
- [13] T. H. Mohamed, M. A. M. Alamin, and A. M. Hassan, "A novel adaptive load frequency control in single and interconnected power systems," *Ain Shams Engineering Journal*, vol. 12, no. 2, pp. 1763–1773, 2021.
- [14] J. Morsali, K. Zare, and M. T. Hagh, "Performance comparison of tsc with tps and sssc controllers in agc of realistic interconnected multi-source power system," *Ain Shams Engineering Journal*, vol. 7, no. 1, pp. 143–158, 2016.

- [15] A. Han, Z. Zhang, X. Yin, J. Zhang, and M. Liang, "Research on fault characteristic and grid connecting-point protection scheme for wind power generation with doubly-fed induction generator." *Transactions of China Electrotechnical Society*, vol. 27, no. 4, pp. 233–239, 2012.
- [16] H. Sun, B. Zhang, J. Wang, D. Sun, J. Tong, K. Moslehi, F. Li, K. Strunz, and F. Li, "Guest editorial distributed energy management systems," *IEEE Transactions on Smart Grid*, vol. 7, no. 2, pp. 971–973, 2016.
- [17] C. Yu, L. Qi, J. Sun, C. Jiang, J. Su, and W. Shu, "Fault diagnosis technology for ship electrical power system," *Energies*, vol. 15, no. 4, p. 1287, 2022.
- [18] Y. Zhang, T. Yang, and Z. Tang, "Active fault-tolerant control for load frequency control in multi-area power systems with physical faults and cyber attacks," *International Transactions on Electrical Energy Systems*, vol. 31, no. 7, p. e12906, 2021.
- [19] G. Yang and Z. Zhang, "Review of fault diagnosis techniques for dynamic systems based on interval observer," *Control and Decision*, vol. 33, no. 33, p. 13, 2017.
- [20] M. R. Davoodi, K. Khorasani, H. A. Talebi, and H. R. Momeni, "Distributed fault detection and isolation filter design for a network of heterogeneous multiagent systems," *IEEE Transactions on Control Systems Technology*, vol. 22, no. 3, pp. 1061–1069, 2013.
- [21] X. Qiu, C. Long, X. Xing, C. Yingfeng, C. Te, and W. Xiaohan, "Fault estimation based fault-tolerant control method for unmanned vehicle," *Transactions of Beijing Institute of Technology*, vol. 42, no. 7, pp. 723–732, 2022.
- [22] Y. Junqi, L. Zechen, C. Lizhi, and X. Jianhao, "Robust actuator fault estimation for a class of disturbed linear sampled data systems," *Control Theory and Applications*, vol. 47, no. 8, pp. 1–7, 2017.
- [23] T. Zhang, X. Zhao, R. Hu, and W. Fu, "A method for fault diagnosis of power system of carrier rocket engine based on linear-quadratic receding time-domain algorithm," *Proceedings of the Institution of Mechanical Engineers, Part G: Journal of Aerospace Engineering*, vol. 236, no. 4, pp. 739–752, 2022.
- [24] K. Zhang, B. Jiang, and P. Shi, "Adjustable parameter-based distributed fault estimation observer design for multiagent systems with directed graphs," *IEEE Transactions on Cybernetics*, vol. 47, no. 2, pp. 306–314, 2016.
- [25] J.-W. Zhu and G.-H. Yang, "Robust distributed fault estimation for a network of dynamical systems," *IEEE Transactions on Control of Network Systems*, vol. 5, no. 1, pp. 14–22, 2016.
- [26] J. Han, X. Liu, X. Gao, and X. Wei, "Intermediate observer-based robust distributed fault estimation for nonlinear multi-agent systems with directed graphs," *IEEE Transactions on Industrial Informatics*, vol. 16, no. 12, pp. 7426–7436, 2019.
- [27] P. P. Menon and C. Edwards, "Robust fault estimation using relative information in linear multi-agent networks," *IEEE Transactions on Automatic Control*, vol. 59, no. 2, pp. 477–482, 2013.
- [28] K. Zhang, B. Jiang, and V. Cocquempot, "Adaptive technique-based distributed fault estimation observer design for multi-agent systems with directed graphs," *IET Control Theory & Applications*, vol. 9, no. 18, pp. 2619–2625, 2015.
- [29] J. Xia, B. Jiang, and K. Zhang, "Dissipativity-based robust reduced-order fault estimation observer design of multi-agent systems," *International Journal of Control, Automation and Systems*, vol. 15, no. 6, pp. 2619–2627, 2017.
- [30] S. Yin, H. Gao, J. Qiu, and O. Kaynak, "Descriptor reduced-order sliding mode observers design for switched systems with sensor and actuator faults," *Automatica*, vol. 76, pp. 282–292, 2017.
- [31] H. Bevrani, *Robust power system frequency control*. New York: Springer, 2014, vol. 4.
- [32] J.-W. Zhu and G.-H. Yang, "Robust distributed fault estimation for a network of dynamical systems," *IEEE Transactions on Control of Network Systems*, vol. 5, no. 1, pp. 14–22, 2016.
- [33] J.-W. Zhu, G.-H. Yang, W.-A. Zhang, and L. Yu, "Cooperative fault tolerant tracking control for multiagent systems: An intermediate estimator-based approach," *IEEE Transactions on Cybernetics*, vol. 48, no. 10, pp. 2972–2980, 2017.
- [34] J.-W. Zhu, G.-H. Yang, H. Wang, and F. Wang, "Fault estimation for a class of nonlinear systems based on intermediate estimator," *IEEE Transactions on Automatic Control*, vol. 61, no. 9, pp. 2518–2524, 2015.